Autonomous System for Vaginal Cuff Closure via Model-Based Planning and Markerless Tracking Techniques

Michael Kam, Shuwen Wei, Justin D. Opfermann, Hamed Saeidi, Michael H. Hsieh, Karen C. Wang, Jin U. Kang, *Member, IEEE*, and Axel Krieger, *Member, IEEE*

***Abstract*—Autonomous robotic suturing has the potential to improve surgical outcomes compared to manual operations due to better accuracy and consistency of suture placement. In this letter, we develop an autonomous system with model-based planning and markerless tissue tracking techniques for autonomous vaginal cuff closure. The proposed planning method constructs an optimal suture plan that minimizes tissue collisions with the robotic suturing tool. Moreover, DeepLabCut is utilized for autonomous markerless soft-tissue tracking in robotic vaginal cuff closure. Furthermore, an instruction-based autonomous surgery interface (ASI) is designed to automate the complex suturing workflow. The proposed planning method is evaluated via a robotics simulator and real-world suture-placement tests. End-to-end vaginal cuff closure via Smart Tissue Autonomous Robot (STAR) on synthetic tissues was carried out and compared to the suturing results via conventional laparoscopic and robot-assisted approaches performed by experienced surgeons. The comparison results indicate that by using the proposed planning pipeline, STAR outperforms conventional laparoscopic and robotic-assisted methods with better accuracy and consistency, thus achieving a higher success rate of autonomous suture placement.**

***Index Terms*—Medical robots and systems, surgical robotics: planning, control architectures and programming.**

I. Introduction

HYSTERECTOMY for gynecologic disease is one of the most common surgical procedures; 1 in 9 women in the United States undergo the procedure during their lifetimes [1].

Manuscript received 2 November 2022; accepted 14 April 2023. Date of publication 5 May 2023; date of current version 17 May 2023. This letter was recommended for publication by Associate Editor F. Ernst and Editor J. Burgner-Kahrs upon evaluation of the reviewers' comments. This work was supported by the National Science Foundation under Award NSF FRR CAREER 2144348. *(Corresponding author: Michael Kam.)*

Michael Kam, Justin D. Opfermann, and Axel Krieger are with the Department of Mechanical Engineering, Johns Hopkins University, Baltimore, MD 21211 USA (e-mail: michael081906@gmail.com; jopferm1@jhu.edu; axel@jhu.edu).

Shuwen Wei and Jin U. Kang are with the Department of Electrical and Computer Engineering, Johns Hopkins University, Baltimore, MD 21211 USA (e-mail: swei14@jhu.edu; jkang@jhu.edu).

Hamed Saeidi is with the Department of Computer Science, University of North Carolina Wilmington, Wilmington, NC 28403 USA (e-mail: saeidih@uncw.edu).

Michael H. Hsieh is with the Department of Urology, Children's National Health System, Washington, DC 20010 USA (e-mail: mhsieh@cnmc.org).

Karen C. Wang is with the Department of Gynecology and Obstetrics, Johns Hopkins Medicine, Baltimore, MD 21287 USA (e-mail: kwang48@jh.edu).

This letter has supplementary downloadable material available at https://doi.org/10.1109/LRA.2023.3273416, provided by the authors.

Digital Object Identifier 10.1109/LRA.2023.3273416

Vaginal cuff closure, a suturing procedure that closes the vaginal incision after removing the uterus, is an essential step of hysterectomy. Between 2007 and 2010, 46.6% patients underwent an abdominal hysterectomy, 20.7% had a vaginal hysterectomy, 28.6% had a laparoscopic procedure, and 4.1% had a robot-assisted hysterectomy [1]. For benign disease, robot-assisted hysterectomy resulted in shorter surgical time and less blood loss compared with laparotomy-based hysterectomy [2]. Robot-assisted surgery (RAS), a type of surgery performed by a surgeon via robotic teleoperation, has been widely performed over the past two decades for operations that are challenging for conventional laparoscopic approaches, including laparoscopic hysterectomy and vaginal cuff closure [1]. However, RAS still requires an operator to control and teleoperate the system, and the surgical outcomes can vary depending on the surgeon's proficiency, training, and surgical experience. To further reduce human error, autonomous RAS aims to integrate more autonomy into the surgical workflow, such as in autonomous suturing. The hypothesis is that with more advanced robotic automation technologies, the autonomous controller can achieve more consistent and accurate suturing outcomes compared to manual suturing.

Efforts in automating robotic suturing range from sub-task development to system-level paradigms. Saeidi et al. demonstrated autonomous in vivo small intestinal anastomoses using Smart Tissue Autonomous Robot (STAR) [3]. The system incorporated an autonomous control strategy for challenging breathing motion and vision constraints in a laparoscopic environment. Jackson et al. focused on needle path planning for autonomous suturing operations in endoscopic surgery with the goal of minimizing interaction forces between the tool and the tissue [4]. Pedram et al. developed a system-level suturing framework consisting of a needle path planner and vision-based needle pose estimator for autonomous suturing via a cable-driven surgical robot [5]. In [6], an optimization-based needle path planning was proposed and implemented to automate multi-throw suturing with the da Vinci Research Kit (dVRK). Lu et al. developed a spatial trajectory planner with dynamic approaches to coordinate two grippers for autonomous knot tying [7]. Knoll et al. developed a 'scaffolded learning' approach to human-machine skill transfer for robotic arms to automate the task of knot-tying [8]. Kam et al. proposed a confidence-based method for suture planning that predicted the success rate in autonomous suturing and suggested manual assistance when necessary to maximize the overall success of

suture placement [9]. Tissue tracking using fiducials was implemented in autonomous suturing to generate and maintain a feasible surgical plan when the soft tissue deforms in the surgery [10]. Recent developments in deep learning methods have demonstrated a superior performance than conventional computer vision approaches in landmark tracking without the need for artificial fiducials such as coordinate regression [11], heatmap regression [12] and graph regression [13].

Despite these technological successes, these studies have several fundamental and system-level limitations that prevent higher levels of autonomy in robotic suturing of soft tissues. First, suture planning techniques using 3D tissue point clouds did not consider collisions between tissue and suturing tools when generating a suture plan. Such open-loop planning leads to a less feasible plan for autonomous suturing and often requires manual re-positioning to avoid suture-placement failure. In [9] for example, an open-loop planner for autonomous suturing with STAR resulted in a failed suture placement rate of 25% (i.e., 13 of 52 all planned stitches). Second, a suture planner with limited degrees-of-freedom (DoF) planning capabilities reduces the success rate of autonomous suture placement. In [3], [9], the planner generated only position waypoints without orientating the suturing tool; therefore, the planning results were less adapted to the deformed tissue. Third, the use of marker-based tissue tracking techniques lacks robustness and autonomy for soft-tissue suture planning. A suture planner requires a sequence of markers' locations to create an initial plan that is continuously updated during the procedure; however, it is challenging to autonomously sort or restore the same sequence of markers via conventional computer vision approaches on a non-rigid deformed object after an occlusion happened (e.g., instruments blocking). Challenges from marker overlapping which leads to planning failures due to insufficient marker counts are also common and remain unsolved. Finally, the focus on surgical robotic systems lack approaches to effectively combine robotic and manual workflows on autonomous suturing as well as to evaluate pointcloud-based suture planning.

In this letter, an autonomous system with comprehensive solutions was proposed for STAR (Fig. 1(a)) for robotic vaginal cuff closure. First, a model-based suture planner with 6-DoF suturing-pose optimization was developed to estimate optimal suture plans for STAR by minimizing collisions between the model of a suturing device and the tissue point cloud, shown in Fig. 1(b). Compared to our prior work in [9], the proposed planning method enables the suture planner to actively refine and search for an optimal suturing pose, thereby improving the success rate in suture placement. Second, a markerless tissue tracker was developed with DeepLabCut[14] integration for real-time soft tissue tracking, shown in Fig. 1(c). Tissue landmarks were tracked to optimize the suture placement and determine re-plan operation in autonomous suturing. Lastly, an autonomous surgery interface (ASI) was developed for STAR for autonomous suturing and allowed operators to supervise the suturing workflow with minimum manual effort. Simulated and suture-placement experiments were carried out to evaluate the proposed planning method and compare results with other planning strategies. End-to-end robotic vaginal cuff closure

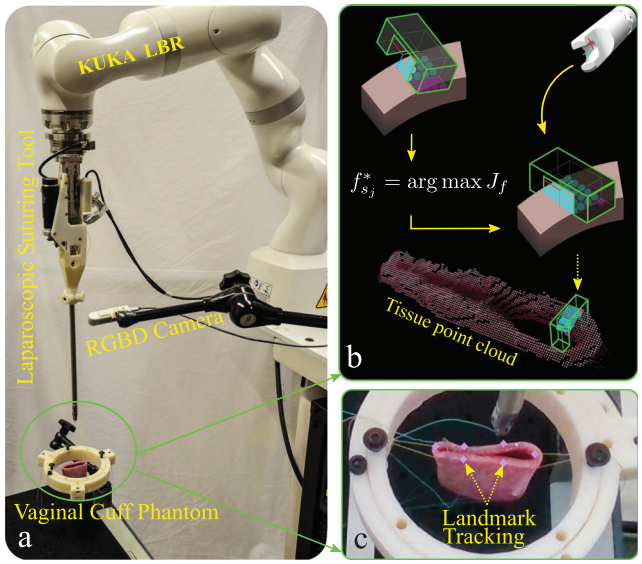

Fig. 1. Autonomous system for robotic vaginal cuff closure: a) experimental setup of STAR, b) model-based suture planning refines the suturing pose of STAR to minimize tissue collisions of the suturing tip, and c) markerless tissue tracker enables real-time landmark tracking for autonomous suturing.

demonstrated the feasibility of ASI and the results were compared to the suturing results via conventional laparoscopic surgery (CLS) and RAS performed by experienced surgeons. The remainder of this letter is organized as follows: the robotic system as well as the planning and tracking methods are detailed in Section II, the test results via the autonomous system are presented in Section III and discussed in Section IV, and Section V concludes the letter.

II. Method

A. Robotic System Setup

The experimental setup for our STAR system is shown in Fig. 1(a). The STAR consists of a 7-DoF KUKA LBR Med lightweight arm (KUKA AG, Augsburg Germany) and a customized laparoscopic suturing tool from EndoEvolution (North Chelmsford, MA, USA). The suturing device was motorized using two DC brush motors (Maxon Motors, Sachseln, Switzerland) to control a circular needle and the pitch motion of the tool tip. The motors were connected to the EPOS2 controllers (Maxon Motors, Sachseln, Switzerland) and were controlled by a host computer via a controller area network (CAN). A multi-axis force sensor (ATI industrial automation, NC, USA) was mounted between the suturing tool and an end-effector to measure tensioning force to prevent tissue from damage during suturing tasks. An RGBD camera, Realsense D415 (Intel Corp., Santa Clara, California), was used as an imaging system to stream images and point cloud for planning and tracking in robotic suturing. The coordinate system of the camera was registered onto the robot coordinate system via hand-to-eye calibration using a 3D-printed rod and a checkerboard. The point cloud w.r.t robot coordinate can be derived via homogeneous transformation and will be used by STAR for vision-guided

suturing tasks. To compensate for the kinematic discrepancy of the suturing tool, a 2 mm z-axis offset (w.r.t. the tool tip) was empirically added to the controller.

B. Autonomous Suturing Workflow

The goal of this work was to perform simulated vaginal cuff closure by using STAR to autonomously place sutures that sufficiently closed the lumen of a synthetic vaginal tissue. The tissue phantom was secured in a stationary 3D-printed ring using two stay sutures (shown in the green circle in Fig. 1(a)), which mimicked the clinical setup of vaginal cuff closure. STAR utilized the 2D images and 3D point cloud from the RGBD camera to perform tissue tracking and generate suturing locations. For each suturing location, STAR controlled the laparoscopic suturing tool and placed a suture on each planned location. A snapshot of the procedure is shown in Fig. 1(c), where STAR placed sutures from the left corner to the right corner of the cuff, and the cuff's lumen was gradually closed by the applied suture tension.

The high-level autonomous workflow of STAR for vaginal cuff closure is described in Algorithm 1. The control workflow of Algorithm 1 was implemented with the robot language of STAR and was executed via the kernel of ASI (detailed in Section II-E). We defined k indicating k^{th} suturing point and k will be increased with every completion of a suture. In Algorithm 1, the kernel first requested tissue landmarks $L \subset \mathbb{R}^3$ of vaginal cuff at timestamp t (i.e., L_t) from markerless tracker (detailed in Section II-D) in line 2. The extracted landmark was utilized to generate suture plan $S \subset \mathbb{R}^3$ via suture path planning (detailed in Section II-C1) in line 3. At every suturing point $s_j \in S$, the model-based optimization was carried out to refine the suturing pose $f^*_{s_j} \in \mathbb{R}^6$ of STAR (detailed in Section II-C2) in line 6. The motion planner of STAR used an optimal suturing pose $f^*_{s_k}$ for k^{th} suturing point to perform suturing subroutine, including linear motion approaching, needle firing, and suture tensioning from line 9 to 11. The suturing subroutine required human approval on each step to avoid the failure of suture placement. For suture tensioning, a maximum tension force of 2 N and a tension distance of 15 cm were set to prevent tearing the tissue. After completion of each suture, the kernel examined the new tissue scene and determined whether a re-plan was needed via comparing the location change of landmarks of L_t and L_{t-1} in line 13. If the location change of landmarks is significant, a re-plan was required to update a new suture plan (i.e., go to line 2); otherwise, the workflow kept the current suture plan and continued to place the next suture (i.e., go to line 9).

C. Model-Based Suture Planning

A model-based suture-planning method was proposed to facilitate STAR for autonomous robotic suturing on vaginal cuff closure. A tool-tip model was developed and the coordinate frame of the model was denoted as $f \in \mathbb{R}^6$ with origin defined at the rotation center of the circular needle, shown in Fig. 2(a). The dimension of the model is the same dimension (10 mm $\times$ 3 mm $\times$ 5 mm) of the needle tip. The suture planning

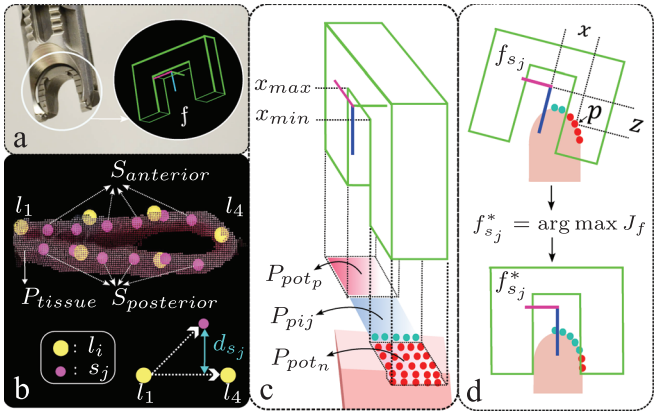

Fig. 2. Concepts of model-based suture planning: a) the proposed tool-tip model in 3D with its coordinate frame f represents the actual tip of the suturing tool, b) suture path planning uses 3D landmarks l_i to generate suturing points s_j on the tissue point cloud, c) proposed tool-tip model with a collected point cloud based on the model geometry, and d) model-based optimization determines optimal pose $f^*_{s_j}$ for each s_j via maximum cost J_f.

Algorithm 1: Autonomous Suturing Workflow.

1: $k = 0$
2: $L_t \leftarrow NewLandmarks$ ▷Markerless Tracking
3: $S \leftarrow NewSutrePlan(L_t)$▷Path Planning
4: $j = 0$
5: **while** $j < S.size()$ **do**
6: $\quad f^*_{s_j} \leftarrow argmaxJ_f$ ▷Model-based Optimization
7: $\quad j \leftarrow j + 1$
8: **end while**
9: $MoveTo(f^*_{s_k})$ ▷STAR Robotic Suturing
10: $NeedleFiring$
11: $Tensioning(f^*_{s_k})$
12: $k \leftarrow k + 1$
13: **if** $Replan(L_t, L_{t-1})$ **then go to 2**
14: **else go to 9**
15: **end if**

consists of suture path planning and model-based optimization to determine f.

1) Suture Path Planning: Suture path planning based on landmark information (e.g., start, midpoint, and end locations) was used to identify the suturing locations along the edges of the synthetic tissue. The set of landmarks L (yellow spheres in Fig. 2(b)), containing $l_i \in \mathbb{R}^3$, was tracked by the tissue tracker on the tissue point cloud (detailed in Section II-D). In this study, six landmarks were needed based on tissue size and our prior experience [9]. The order of l_i was defined as starting from the left most landmark and increased sequentially in a clockwise direction. The point cloud of the target tissue is denoted as P_{tissue} which is generated via the depth camera. Dijkstra algorithm [15] was utilized to compute trajectories on anterior and posterior edges of the P_{tissue} from l_1 to l_4. An equal-spacing algorithm was applied to find equally spaced point sets $S_{anterior}$ and $S_{posterior}$ on each corresponding trajectory. We defined S as the union of $S_{anterior}$ and $S_{posterior}$ which contains suturing point $s_j \in S \subset \mathbb{R}^3$ (pink spheres in Fig. 2(b)).

Least-square plane fitting was applied to S to find an accurate approximation for the surface of the cuff's lumen. We defined f_{s_j} for the model at each suture point s_j, and the orientation of f_{s_j} was constructed with two bases: the normal of the best-fitted plane of S and a vector pointed toward s_{j+1} in each subset (e.g., $S_{anterior}$ or $S_{posterior}$). The normal of the best-fitted plane of S defines the z-axis of f_{s_j} (i.e., the blue axis of f), and the vector pointed toward s_{j+1} defines the y-axis of f_{s_j} (i.e., the green axis of f).

2) Model-Based Optimization: The tool-tip model optimized and adjusted each f_{s_j} to an optimal location $f^*_{s_j}$ that maximizes the success rate for the suture placement. The model collected $P_{tool} \subset P_{tissue}$ within the model's boundary w.r.t f_{s_j}. The origin of the tool-tip model f_{s_j} was configured on a s_j, and P_{tool} was categorized into three subsets along the x-axis of the model, illustrated in Fig. 2(c). A point located between $x_{\max}$ and $x_{\min}$ is labeled as point-in-jaw and belongs to a set P_{pij}, where $x_{\max}$ is at $+2.5$ mm and $x_{\min}$ is at -2.5 mm w.r.t f_{s_j} along x-axis. A set of points in the model beyond $x_{\max}$ is defined as the point-on-tool-positive P_{pot_p}. A set of points in the model below $x_{\min}$ is defined as the point-on-tool-negative P_{pot_n}. In addition, P_{pot} is defined as the union of P_{pot_p} and P_{pot_n}. The (1) and (2) were applied to compute the weight for each of the point $p \in P_{tool}$ based on the x and z coordinate of p w.r.t f_{s_j}, illustrated in the top figure of Fig. 2(d)

$$w(x,z) = b(x) \cdot \frac{1}{\sigma(z+\mu)} \tag{1}$$

$$b(x) = \begin{cases} (x_{\min} - x), & x < x_{\min} \\ (x - x_{\max}), & x > x_{\max} \\ \frac{x_{\max} - x_{\min}}{2}, & \text{otherwise} \end{cases} \tag{2}$$

where $\sigma > 0$ and $\mu > 0$. In this study, σ and μ were set to 5 and 0.001, respectively. If p is further away from the f_{s_j} along the z-axis, $h(z)$ reduces the weight of such point. If p is the element of P_{pot_p} or P_{pot_n}, $b(x)$ increases the weight when the point is further away from the boundary (e.g., $x_{\max}$ or $x_{\min}$), and vice versa. The total weight of a subset is the summation of weights computed in that subset (e.g., $W_{pij} = \Sigma_{P_{pij}} w(x,z)$, $W_{pot_p} = \Sigma_{P_{pot_p}} w(x,z)$, and $W_{pot_n} = \Sigma_{P_{pot_n}} w(x,z)$). We defined J_f as the cost of the model at f, and $J_{f_{s_j}}$ as the cost of the model at f_{s_j} via (3)

$$J_{f_{s_j}} = \mathbf{W_{f_{s_j}}}^{\intercal} \mathbf{G_{s_j}} \tag{3}$$

where $\mathbf{W_{f_{s_j}}} = [W_{pij} \quad W_{pot_p} \quad W_{pot_n}]^{\intercal} \in \mathbb{R}^3$ and $\mathbf{G_{s_j}} = [G_{pij} \; G_{pot_p} \; G_{pot_n}]^{\intercal} \in \mathbb{R}^3$. $\mathbf{W_{f_{s_j}}}$ can be viewed as the virtual force applied from the tissue point cloud to the tool-tip model at the pose of f_{s_j}. W_{pij} represents the virtual force that allows a collision-free approach of the tool-tip model, while W_{pot_p} and W_{pot_n} represent the virtual forces that resist the tool-tip model at f_{s_j}. Since the goal was to find the f_{s_j} that maximizes the success rate for suture placement at each s_j, a discrete optimization was carried out to search for $f^*_{s_j}$ that maximizes the allowing virtual force and minimizes the resisting virtual forces via (4)

$$f^*_{s_j} = \underset{f \in U(f_{s_j})}{\operatorname{argmax}} J_f \tag{4}$$

where $U(f_{s_j})$ is a finite set contains various configurations based on f_{s_j}. Fig. 2(d) shows the concept of the optimization where the optimal $f^*_{s_j}$ was determined by traversing through the $U(f_{s_j})$ and finding maximum J_f. In this study, the finite set $U(f_{s_j})$ was the combination of translation on the x-axis and rotation on the y-axis of the f_{s_j}.

In vaginal cuff closure, the area of the cuff's lumen will be gradually reduced as each suture brings the anterior and posterior edges of the cuff together until the two edges are eventually sealed by the tension of the final suture. Therefore, the configuration of the tissue was also considered in the optimization process. We defined proximity d_{s_j} for each s_j, shown in Fig. 2(b), via (5)

$$d_{s_j} = \left\| \mathbf{v_{s_j}} - \frac{\mathbf{v_l} \cdot \mathbf{v_{s_j}}}{\mathbf{v_l} \cdot \mathbf{v_l}} \mathbf{v_l} \right\|_2 \tag{5}$$

where $\mathbf{v_l} \in \mathbb{R}^3$ is the vector from the start to the end landmarks (i.e., l_1 and l_4), $\mathbf{v_{s_j}} \in \mathbb{R}^3$ is the vector from l_1 to s_j, and $\| \; \|_2$ denotes as Euclidean norm.

Next, a parameter ρ was defined as a threshold for determining tissue configuration and was specified prior to the suturing procedure. If the d_{s_j} is less than ρ, we considered the tissue as closed configuration at s_j, and vice versa. In this study, ρ was set to 5 mm based on thickness of the edge of the tissue phantom. The $\mathbf{G_{s_j}}$ was determined via (6) in this study

$$\mathbf{G_{s_j}} = \begin{cases} [1 \; -1 \; -1]^{\intercal}, & d_{s_j} > \rho \\ [1 \; -5 \; \; 0]^{\intercal}, & d_{s_j} < \rho, \; s_j \in S_{anterior} \\ [1 \; \; 0 \; -5]^{\intercal}, & d_{s_j} < \rho, \; s_j \in S_{posterior} \end{cases} \tag{6}$$

where if a s_j is with an open configuration (Fig. 1(b)), both W_{pot_p} and W_{pot_n} are taken in the optimization process; however, if the s_j is with a closed configuration, the process will only consider either W_{pot_p} or W_{pot_n}. The negative sign of $\mathbf{G_{s_j}}$ indicates both W_{pot_p} and W_{pot_n} were penalty terms that intend to reduce the J_f. The optimization searched for $f^*_{s_j}$ in which the tool-tip model contains the largest W_{pij} but smallest W_{pot_p} and W_{pot_n} to maximize the success rate for the suture placement.

D. Markerless Tissue Tracking

We utilized DeepLabCut [14] to track tissue landmarks on image frames. DeepLabCut is a deep convolutional network which incorporates variations of deep residual neural networks (ResNet) [16] from DeeperCut [17] and deconvolutional layers for feature recognition. The landmark location was predicted by finding the peak of the corresponding probability score-maps [14] of the network output. In this study, a variant of ResNet with 50 layers was selected as the network type with pre-trained weights on ImageNet database [18]. We fine-tuned the network by minimizing the cross-entropy loss between the score-maps of prediction and ground-truth labeled via DeepLabCut toolbox [19]. Fig. 3(a) shows an example of the labeled 2D location of landmarks in which l_1 and l_4 were labeled at the left and right end of the tissue, l_2 and l_3 were labeled on the anterior edge, and l_5 and l_6 were labeled on the posterior edge. Landmarks labeled on anterior and posterior were spaced equally in the distance

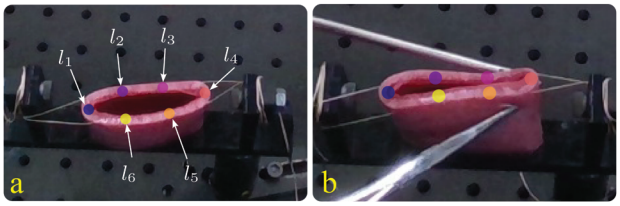

Fig. 3. a) 2D landmarks labeled on a synthetic cuff tissue via DeepLabCut toolbox; b) labeled image of deformed cuff tissue using tweezers.

between l_1 and l_4. Deformation was manually applied to tissue samples to simulate the cuff closure in the surgical process, as shown in Fig. 3(b). We fine-tuned the network offline using total of 120 labeled images with data augmentation performed in 30,000 training steps and found the test error to be 3.69 pixels.

A markerless tracker computed the real-time 3D coordinates of the 2D landmarks as predicted by the trained DeepLabCut model during the robotic suturing tasks. The 3D coordinate of l_i was determined by finding closest projected tissue point cloud on the 2D location of the tracked landmarks, given intrinsic and extrinsic camera parameters. The constant order of l_i was continuously maintained by the tracker, which plays a key role in re-plan operation of suture planning. Moreover, the tracker computed the magnitude of position change of landmarks via (7)

$$D_k = \frac{1}{m}\sum_{i=1}^{m} \|l_i^k - l_i^{k-1}\|_2 \tag{7}$$

where k is the timestamp and m is the total number of landmarks. D_k indicates the level of tissue deformation and an update for the suture plan is needed if D_k exceeds a preset threshold γ, i.e,. $D_k > \gamma$. In this study, γ was set to 5 mm.

E. Software Architecture

An ASI was developed for STAR with software architecture shown in Fig. 4(a) and was integrated into the Robot Operating System (ROS). A graphical user interface (GUI) was developed for an operator to control and monitor the robotic system. The GUI is split into two operating sections for control under manual and auto modes. In the manual mode, the operator controls the action of the robotic system via GUI such as tool-tip re-positioning, needle firing, and teach-point recording. The design of the GUI shares the commonality of an industrial robot controller in which three types of motion control are provided: joint, Cartesian, and tool. In auto mode, the GUI executes a script-based pre-plan workflow autonomously created by the operator. We implemented a programmable language on ASI via the patterns of regular expression for building primitive task commands, including motion control, basic arithmetic, path planning, logic operator, etc. The autonomous workflow is constructed by combining multiple task commands sequentially in a single script file. An interpreter was built to translate task commands in the script and display the contents of the entire workflow to the GUI. The progress of the autonomous workflow is shown on the GUI to allow human supervision and workflow control (e.g., start, pause, stop, etc.).

The system architecture of ASI was designed with distributed infrastructure to facilitate system-level implementation. The system architecture contains modules for designated subtasks such as suture planning, motion execution, markerless tracking, force sensing, etc. In addition, a kernel was developed to control the process workflow in a centralized manner. In auto mode, the kernel mapped each command in the autonomous workflow to a corresponding request and sent it to a specific module for task execution via synchronous service of ROS. Such remote procedure call (RPC) request and reply interactions allow better tracing of the state transition in the autonomous workflow. Moreover, the kernel handles errors by checking the reply from each module and will pause the autonomous workflow if an error was raised.

F. Experimental Design and Evaluation Criteria

The hypothesis of this study is that the use of ASI with new planning and tracking techniques will improve the suturing results of robotic vaginal cuff closure with more consistent suture placement and fewer missed sutures. Three experiments were carried out to systematically test the hypothesis via 1) planning evaluation framework, 2) suture-placement test, and 3) robotic vaginal cuff closure. The planning evaluation framework tests the method of model-based suture planning on simulated tissue. The suture-placement test evaluates the model-based suture planning on vaginal cuff tissue phantoms with STAR. The robotic vaginal cuff closure evaluates end-to-end suturing results via ASI using model-based suture planning and markerless tracking techniques on vaginal cuff tissue phantoms.

1) Planning Evaluation Framework: A simulator was built to evaluate different suture planning methods. A mock STAR was built using Gazebo with ROS and was controlled by ASI with the same hardware interface of the real robot, illustrated in Fig. 4(b). Moreover, a simulated depth camera and model of cuff tissue were integrated into the simulator. The model of cuff tissue was created using SOLIDWORKS with the same geometrical dimension as a real cuff tissue phantom. The shape of the model of cuff tissue was made via observing images in our previous experiments [9]. Different tissue shapes and surfaces were taken into account for model creation. The camera in the virtual environment, with the identical camera parameters as the D415, extracted 2D and 3D of its field of view, shown in Fig. 4(c). Landmarks on each model of cuff tissue were defined via the CAD and were used to perform suture path planning on tissue point cloud generated by the simulated camera. The model of cuff tissue was imported into the simulator and was taken to evaluate suture planning methods.

2) Suture-Placement Test: We utilized STAR to perform suture-placement tests to evaluate whether the planning result via the model-based suture planning is feasible and with sufficient accuracy in a real-world scenario. Dry synthetic vaginal cuff tissue (3-Dmed, Ohio, United States) was chosen with 5 cm diameter and 5 mm wall thickness for the suture-placement tests.

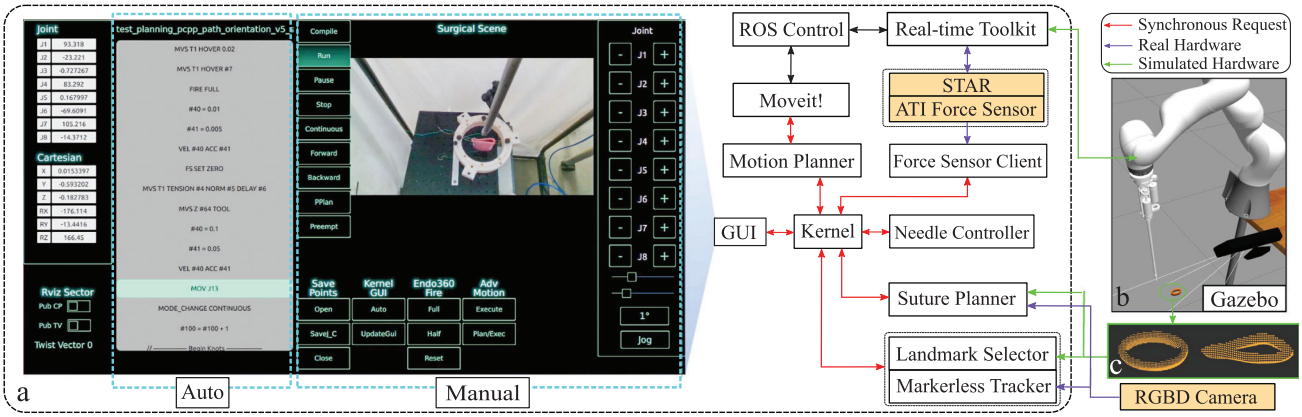

Fig. 4. Software architecture of the autonomous system with a) autonomous surgery interface, b) planning evaluation framework via Gazebo with tissue model, and c) tissue point cloud generated from the simulated camera.

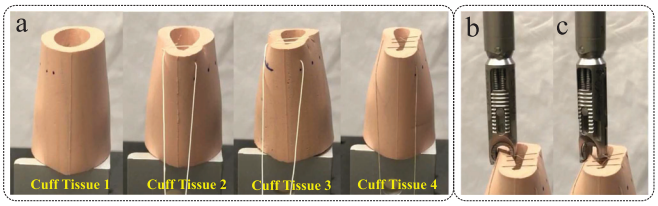

Fig. 5. a) Four tissue configurations used in the suture-placement test to evaluate suture planning methods, and examples of b) success and c) failure in suture-placement.

The cuff tissue was placed on a stand located in front of the camera with a distance of 45 cm which satisfies the minimum sensing distance of the RGBD camera. To avoid collision with STAR, the camera was placed off axis at a viewing angle of 10-13° w.r.t. the vaginal cuff's lumen. In total four tissue configurations were chosen in the test, shown in Fig. 5(a), including tissue with no sutures, two sutures, four sutures, and six sutures placed. For each tissue configuration, STAR performed suture-placement tests via either 1) model-based suturing planning or 2) suture planning [9], and the results were compared and evaluated. Because the suture planning in [9] does not involve orientation planning, the tool-tip's rotation was fixed so that the x-axis of f was orthogonal to the linearization of cuff tissue (i.e., $\mathbf{v_1}$). STAR performed suture-placement tests via a modified workflow of Algorithm 1 and reached each suture location s_k without firing the needle nor re-plan operation. The landmarks l_i were selected prior to the test and STAR only tested the location in which no physical suture was placed. Success was defined as the jaw of the suturing tool fits in the edge of the cuff tissue (Fig. 5(b)) and a failure was determined if the edge of the cuff tissue does not fit into the jaw of the suturing tool (Fig. 5(c)). We compared the results on the percentage of success reaching the s_k and the average cost J_f estimated by suture planners.

3) Robotic Vaginal Cuff Closure: For system evaluation, we utilized STAR to perform end-to-end cuff closure on wet synthetic vaginal cuff tissue with setup shown in Fig. 1(a). The suturing results performed by STAR via ASI were compared to the results of CLS [9] and RAS performed by an experienced surgeon via daVinci SI system. The results were compared on i) suture spacing (i.e., the distance between consecutive suture-entry locations) and ii) bite size (i.e., the shortest distance from suture-entry location to the cross-sectional surface of tissue). The two measures are relevant to post-surgical complications such as infection and dehiscence [20]. Statistical analysis with Levene's test was carried out to evaluate the variances of suture spacing and bite size. A student's t-test was used for comparison of means between different groups. Bonferroni correction was applied to counteract the effects of multiple comparisons and the corrected significance level α for all statistics became $\alpha = 0.0167$. Moreover, we compared the results of STAR in this study to our prior work [9] on the percentage of human intervention in suture placement.

III. Results

A. Results of Planning Evaluation

We evaluated the model-based suture planning via the planning evaluation framework. Fig. 6 shows the planning results on models of cuff tissue via the workflow of Algorithm 1 from line 2 to 8. Four different shapes of cuff tissue were selected to simulate cuff closure in the suturing process. The results of suture planning via model-based suture planning with corresponding models of cuff tissue are shown in Fig. 6(a), Fig. 6(b), Fig. 6(c), and Fig. 6(d). The planning results via suture planning [9] with corresponding models of cuff tissue are shown in Fig. 6(e), Fig. 6(f), Fig. 6(g), and Fig. 6(h). In each figure of the planning result, P_{pij} are in cyan color and P_{pot} are in pink color. The results show that the model-based suture planning generated more feasible suture plans where the y-axis of each tool-tip model is approximately the tangent of the edge contour on each model of cuff tissue, and the pose of the tool-tip model was optimized with most P_{pij} and least P_{pot}. In comparison, the suture plan generated by the suture planning method [9] kept the same orientation across all suture points, which could lead to a suture-placement failure at some locations where the edge profile of the cuff tissue does not properly align with the suturing tip (e.g., suture points in the left corner of the cuff tissue in Fig. 6(e)). Fig. 6(i) shows the average J_f of the planning

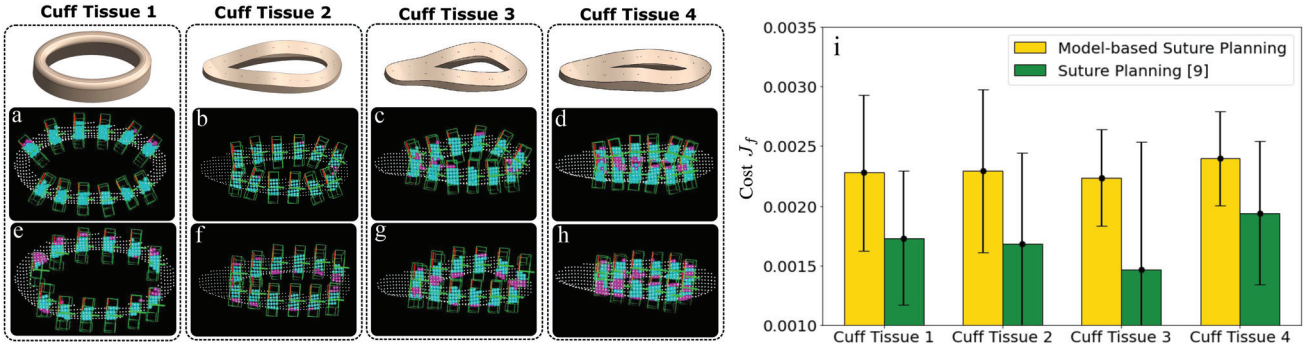

Fig. 6. Planning results via model-based suture planning with four models of cuff tissue are shown in simulation in (a), (b), (c), and (d); planning results via suture planning [9] are shown in (e), (f), (g), and (h); (i) average cost J_f estimated by the suture planning [9].

TABLE I
COMPARISON OF RESULTS OF THE SUTURE-PLACEMENT TEST

Number of success/Number of attempt (Average Cost J_f)		
Planning method / Tissue model	Model-based suture planning method	Suture planning method [9]
Cuff Tissue 1	12/12 (0.0096)	6/12 (0.0065)
Cuff Tissue 2	10/10 (0.0107)	6/10 (0.0056)
Cuff Tissue 3	8/8 (0.0100)	7/8 (0.0089)
Cuff Tissue 4	5/6 (0.0099)	5/6 (0.0088)
Total	35/36	24/36
Success Rate	**97%**	**66%**

TABLE II
COMPARISON OF RESULTS OF VAGINAL CUFF CLOSURE

Metric / Modality	Suture spacing (mm)	Bite size (mm)	Manual-adjusting rate (miss/attempt sutures)
STAR	$7.11 \pm \mathbf{0.81}$	$7.0 \pm \mathbf{0.71}$	**1/48**
RAS	6.54 ± 1.467	7.11 ± 1.163	–
CLS [9]	9.19 ± 2.08	4.96 ± 2.39	–
STAR [9]	7.41 ± 1.33	5.71 ± 1.34	13/52

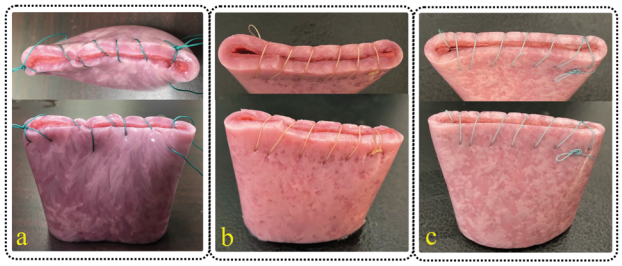

Fig. 7. Representative results of synthetic vaginal cuff closure via a) CLS, b) RAS, and c) STAR with model-based suture planning.

results via the model-based suture planning method and suture planning method [9] on each model of cuff tissue.

B. Results of Suture-Placement Test

Table I shows the results of suture-placement test in which two planning strategies were applied to four configurations of cuff tissue, respectively, followed by guiding STAR to reach planned suture points. The table shows that STAR utilized the method of model-based suture planning to reach 35 planned locations out of 36, with a success rate of 97%. The results with using previous STAR's suture planning method [9] had a success rate of 66%. Table I displays the average of J_f from different planning results on each configuration of cuff tissue. The planning result via model-based suture planning method with higher J_f contributes to a high success rate of reaching suture location whereas J_f remains low for suture planning method [9]. The results of the suture-placement test confirm that the method of model-based suture planning improves the success of suture placement.

C. Results of Vaginal Cuff Closure

STAR performed four autonomous vaginal cuff closures via ASI on tissue phantoms. In addition, four RAS results were carried out by an experienced surgeon using the da Vinci surgical system. The suturing results of STAR were compared to results of RAS results and CLS [9], and are summarized in Table II with representative samples shown in Fig. 7. In Table II, the variance of both suture spacing and bite size of STAR are significantly less compared to both CLS ($p < 0.001$ for suture spacing and $p < 0.001$ for bite size) and RAS results ($p < 0.001$ for suture spacing and $p < 0.001$ for bite size). The comparison shows the model-based suture planning method enables STAR to place uniform running sutures with better consistency (3.4 times more consistent than CLS and 1.81 times more consistent than RAS) and consistent bite depth (4.5 times more consistent than CLS and 1.64 times more consistent than RAS). The table shows that the results carried out by STAR via ASI for cuff closure outperformed surgeons in both CLS and RAS approaches.

We compare the robotic results via ASI to the robotic results in a previous study [9]. As seen in Table II, ASI improves STAR to achieve statistically less variance in both suture spacing (1.64 times better) and bite size (1.88 times better) compared to the robotic results in the previous study ($p < 0.001$ for suture spacing and $p < 0.001$ for bite size). Moreover, we compare the manual-adjusting rate (i.e., how many sutures required manual re-position) between two robotic experiments. Table II shows that STAR placed sutures with a higher level of autonomy (97.7%) via ASI, compared to the results in the previous study (75%). The only suture that required manual adjustment in this study was because the tissue was deformed into a shape with a folded edge, which was physically impossible for the needle to

place the suture correctly without manual re-position. The comparison shows that ASI increases the success rate of autonomous suture placement with less need for manual re-position.

IV. Discussion

STAR with the developed ASI demonstrates high accuracy and autonomy of suturing for vaginal cuff closure. Model-based suture planning and markerless tracking contribute significantly to improved consistency of suture spacing and bite depth in robotic results. As demonstrated in this letter, the resulting suturing had less suture-placement failure and fewer instances of manual tool re-positioning. While these results indicate that STAR with ASI achieves higher autonomy in autonomous suturing, we acknowledge that the positioning accuracy of STAR and the performance of the model-based suture planning could be further improved by either identifying a precise kinematic model of the suturing tool via calibration using an optical tracking system, or by integrating a better imaging system. For instance, the D415 camera in this study required a 45 cm sensing distance w.r.t. the tissue and achieved a resolution of 0.45 mm/pixel with $\pm 1\%$ x-y accuracy and $\pm 2\%$ depth accuracy. Because the thickness of the synthetic vaginal cuff was 5 mm, we could generate 11 pixel and voxel representations which was sufficient. However, if a thinner synthetic tissue was used, the performance of the model-based optimization might be compromised due to a more sparse 3D point cloud along the tissue edges. For instance, it may be difficult to suture synthetic small bowel with the setup described in this letter, because the small bowel tissue thickness (< 2 mm) would result in a 60% decrease in the 3D point cloud along the tissue edge. To enable the suturing of thinner walled tissues in future studies, we can use either an Intel Realsense D405 camera that has a 7 cm sensing distance and a resolution of 0.19 mm/pixel, or apply a structured light illumination technique as in [21] to achieve 0.008 mm depth accuracy.

V. Conclusion

We presented an autonomous surgery interface (ASI) incorporated model-based suture planning and markerless tissue tracking techniques to enable STAR to perform autonomous suturing tasks. Specifically, the planning method constructs an optimal suture plan by optimizing the tissue point cloud collected in the tool tip model. The markerless tracker enables continuous soft-tissue tracking as well as supplying information on tissue deformation to improve the accuracy of the suture plan. The ASI facilitates an operator to perform robotic suturing via STAR. The suturing results via ASI show that STAR can achieve a large portion of autonomous workflow and accurate suture placement with the least need for position adjustment from an operator. Moreover, STAR achieves results with better consistency in suture spacing and bite size compared to the approaches of conventional laparoscopy and robot-assisted surgery. Future work includes improving the performance of markerless tracker in a more complicated surgical scene and planning accuracy via integrating an advanced 3D camera system.

References

[1] J. D. Wright et al., "Robotically assisted vs laparoscopic hysterectomy among women with benign gynecologic disease," *JAMA*, vol. 309, no. 7, pp. 689–698, Feb. 2013.

[2] B. B. Albright et al., "Robotic versus laparoscopic hysterectomy for benign disease: A systematic review and meta-analysis of randomized trials," *J. Minimally Invasive Gynecol.*, vol. 23, no. 1, pp. 18–27, Jan. 2016.

[3] H. Saeidi et al., "Autonomous robotic laparoscopic surgery for intestinal anastomosis," *Sci. Robot.*, vol. 7, no. 62, Jan. 2022, Art. no. eabj2908.

[4] R. C. Jackson and M. C. Çavuşoğlu, "Needle path planning for autonomous robotic surgical suturing," in *Proc. IEEE Int. Conf. Robot. Automat.*, 2013, pp. 1669–1675.

[5] S. A. Pedram, C. Shin, P. W. Ferguson, J. Ma, E. P. Dutson, and J. Rosen, "Autonomous suturing framework and quantification using a cable-driven surgical robot," *IEEE Trans. Robot.*, vol. 37, no. 2, pp. 404–417, Apr. 2021.

[6] S. Sen, A. Garg, D. V. Gealy, S. McKinley, Y. Jen, and K. Goldberg, "Automating multi-throw multilateral surgical suturing with a mechanical needle guide and sequential convex optimization," in *Proc. IEEE Int. Conf. Robot. Automat.*, 2016, pp. 4178–4185.

[7] B. Lu, H. K. Chu, K. C. Huang, and L. Cheng, "Vision-based surgical suture looping through trajectory planning for wound suturing," *IEEE Trans. Automat. Sci. Eng.*, vol. 16, no. 2, pp. 542–556, Apr. 2019.

[8] A. Knoll, H. Mayer, C. Staub, and R. Bauernschmitt, "Selective automation and skill transfer in medical robotics: A demonstration on surgical knot-tying," *Int. J. Med. Robot. Comput. Assist. Surg.*, vol. 8, no. 4, pp. 384–397, Dec. 2012.

[9] M. Kam, H. Saeidi, M. H. Hsieh, J. U. Kang, and A. Krieger, "A confidence-based supervised-autonomous control strategy for robotic vaginal cuff closure," in *Proc. IEEE Int. Conf. Robot. Automat.*, 2021, pp. 12261–12267.

[10] S. Leonard, A. Shademan, Y. Kim, A. Krieger, and P. C. W. Kim, "Smart tissue anastomosis robot (STAR): Accuracy evaluation for supervisory suturing using near-infrared fluorescent markers," in *Proc. IEEE Int. Conf. Robot. Automat.*, 2014, pp. 1889–1894.

[11] J. Lu, A. Jayakumari, F. Richter, Y. Li, and M. C. Yip, "SuPer Deep: A surgical perception framework for robotic tissue manipulation using deep learning for feature extraction," in *Proc. IEEE Int. Conf. Robot. Automat.*, Mar. 2021, pp. 4783–4789.

[12] S. Wei et al., "Deep point cloud landmark localization for fringe projection profilometry," *J. Opt. Soc. Amer. A*, vol. 39, no. 4, pp. 655–661, Apr. 2022.

[13] X. Du et al., "Articulated multi-instrument 2-D pose estimation using fully convolutional networks," *IEEE Trans. Med. Imag.*, vol. 37, no. 5, pp. 1276–1287, May 2018.

[14] A. Mathis et al., "DeepLabCut: Markerless pose estimation of user-defined body parts with deep learning," *Nature Neurosci.*, vol. 21, no. 9, pp. 1281–1289, Sep. 2018.

[15] E. W. Dijkstra, "A note on two problems in connexion with graphs," *Numerische mathematik*, vol. 1, no. 1, pp. 269–271, 1959.

[16] K. He, X. Zhang, S. Ren, and J. Sun, "Deep Residual Learning for Image Recognition," in *Proc. IEEE Conf. Comput. Vis. Pattern Recognit.*, Dec. 2015, pp. 770–778.

[17] E. Insafutdinov, L. Pishchulin, B. Andres, M. Andriluka, and B. Schiele, "DeeperCut: A deeper, stronger, and faster multi-person pose estimation model," in *Proc. Eur. Conf. Comput. Vis.* Nov. 2016, pp. 34–50.

[18] A. Krizhevsky, I. Sutskever, and G. E. Hinton, "ImageNet Classification With Deep Convolutional Neural Networks," in *Proc. 25th Int. Conf. Neural Inf. Process. Syst.*, 2012, pp. 1097–1105.

[19] T. Nath, A. Mathis, A. C. Chen, A. Patel, M. Bethge, and M. W. Mathis, "Using DeepLabCut for 3D markerless pose estimation across species and behaviors," *Nature Protoc.*, vol. 14, no. 7, pp. 2152–2176, Jul. 2019.

[20] D. Millbourn, Y. Cengiz, and L. A. Israelsson, "Effect of stitch length on wound complications after closure of midline incisions: A randomized controlled trial," *Arch. Surg.*, vol. 144, no. 11, pp. 1056–1059, Nov. 2009.

[21] H. N. D. Le et al., "Demonstration of a laparoscopic structured-illumination three-dimensional imaging system for guiding reconstructive bowel anastomosis," *J. Biomed. Opt.*, vol. 23, no. 5, May 2018, Art. no. 0 56009.